nature chemistry

ARTICLES

https://doi.org/10.1038/s41557-019-0216-y

Non-chemisorbed gold–sulfur binding prevails in self-assembled monolayers

Michael S. Inkpen[1*], Zhen-Fei Liu[2], Haixing Li[1], Luis M. Campos[3], Jeffrey B. Neaton[2] and Latha Venkataraman[1,3*]

Gold–thiol contacts are ubiquitous across the physical and biological sciences in connecting organic molecules to surfaces. When thiols bind to gold in self-assembled monolayers (SAMs) the fate of the hydrogen remains a subject of profound debate—with implications for our understanding of their physical properties, spectroscopic features and formation mechanism(s). Exploiting measurements of the transmission through a molecular junction, which is highly sensitive to the nature of the molecule–electrode contact, we demonstrate here that the nature of the gold–sulfur bond in SAMs can be probed via single-molecule conductance measurements. Critically, we find that SAM measurements of dithiol-terminated molecular junctions yield a significantly lower conductance than solution measurements of the same molecule. Through numerous control experiments, conductance noise analysis and transport calculations based on density functional theory, we show that the gold–sulfur bond in SAMs prepared from the solution deposition of dithiols does not have chemisorbed character, which strongly suggests that under these widely used preparation conditions the hydrogen is retained.

Following seminal reports in the 1980s[1,2], self-assembled monolayers (SAMs) of thiols on planar metal surfaces, as well as those involved at other interfaces such as nanoclusters, have been the subject of thousands of studies summarized across many substantial reviews[3,4]. The widespread, multidisciplinary interest in such systems stems from their ease of preparation, the commercial availability of appropriate assembly components and the broad scope of utility for nanoscale arrays of self-organized organic molecules. Such SAMs have been studied with myriad techniques, most notably contact goniometry[5], X-ray photoelectron spectroscopy (XPS)[5,6], surface electrochemistry[7], scanning tunnelling microscope (STM) imaging[8], thermal desorption[9] and density functional theory (DFT) calculations[6]. The apparent similarities between SAMs formed from monothiols and disulfides[5], thermal desorption of mixed disulfides from multicomponent SAMs[9] and reductive desorption features in surface cyclic voltammograms[7] provided early impetus to characterize the nature of interfacial bonding in these systems as chemisorbed (sometimes referred to as, but not necessarily synonymous with, binding via a covalent or 'gold–thiolate' interaction); however, multiple studies have since worked to clarify the true nature of this interaction[3,4,10–12]. In concert with this assertion, it has generally been assumed that the hydrogen is lost during the formation of a gold–sulfur bond rather than being retained on the sulfur. This distinction has important implications for our fundamental understanding of the physical properties, spectroscopic features and formation mechanism(s) of thiol-based SAMs. Despite strong notions otherwise, to date it has not been possible to consistently distinguish the protonation state of the gold–sulfur bond in a SAM. Neither surface sensitive probes (for example XPS and surface electrochemistry) nor nanoparticle X-ray diffraction studies can characterize the exact nature of the bond or determine the fate of the hydrogen atom attached to the sulfur under ambient conditions[13].

In parallel to investigations into the fundamental properties of SAMs, thiol linkers have been used extensively to create nanoscale devices in which molecular backbones are electronically and physically connected between gold electrodes[14–19]. Often, such measurements are aimed at understanding structure–function relations across different molecular components. Here, we utilize the electronic conductance signature of single-molecule junctions to determine the nature of the gold–sulfur bonding interaction. We apply the STM break junction (STM-BJ) technique[14,20] to systematically study a series of aliphatic and aromatic molecules comprising different sulfur-based linker groups, in both SAMs and in solutions (see Methods for full details). The measurements involve repeatedly forming and then breaking point contacts between a gold STM tip and substrate while recording the conductance (G = current/voltage) as a function of tip–substrate displacement to generate a conductance trace. These conductance–displacement traces show steps around integer multiples of the conductance quantum G_0 ($=2e^2/h$, where e is the elementary charge and h is Planck's constant) and, in the presence of molecules that can bridge the gap, additional steps at a lower conductance due to the formation of a molecular junction. Thousands of conductance traces are compiled into histograms in which the individual steps add together to form peaks that represent the most probable junction conductance. Critically, our study shows that in gold–thiol SAMs formed from dithiol precursors, the gold–sulfur interfacial coupling is through a physisorbed interaction and not a chemisorbed one. This is in stark contrast to the accepted view and strongly suggests that in SAMs formed from solution deposition the thiol hydrogen is retained.

Results and discussion

Conductance measurements. We first present conductance histograms obtained from STM-BJ measurements for 1,12-dodecanedithiol, $\mathbf{C_{12}(SH)_2}$ (Fig. 1a). Here we observe striking differences depending on whether the data are obtained from (1) 'solution measurements', performed after adding a 0.1 mM solution of $\mathbf{C_{12}(SH)_2}$ in 1,2,4-trichlorobenzene to clean gold electrodes or (2) 'SAM

[1]Department of Applied Physics, Columbia University, New York, NY, USA. [2]Molecular Foundry, Lawrence Berkeley National Laboratory and Department of Physics, University of California, Berkeley, Berkeley, CA, USA. [3]Department of Chemistry, Columbia University, New York, NY, USA.
*e-mail: inkpen@usc.edu; lv2117@columbia.edu

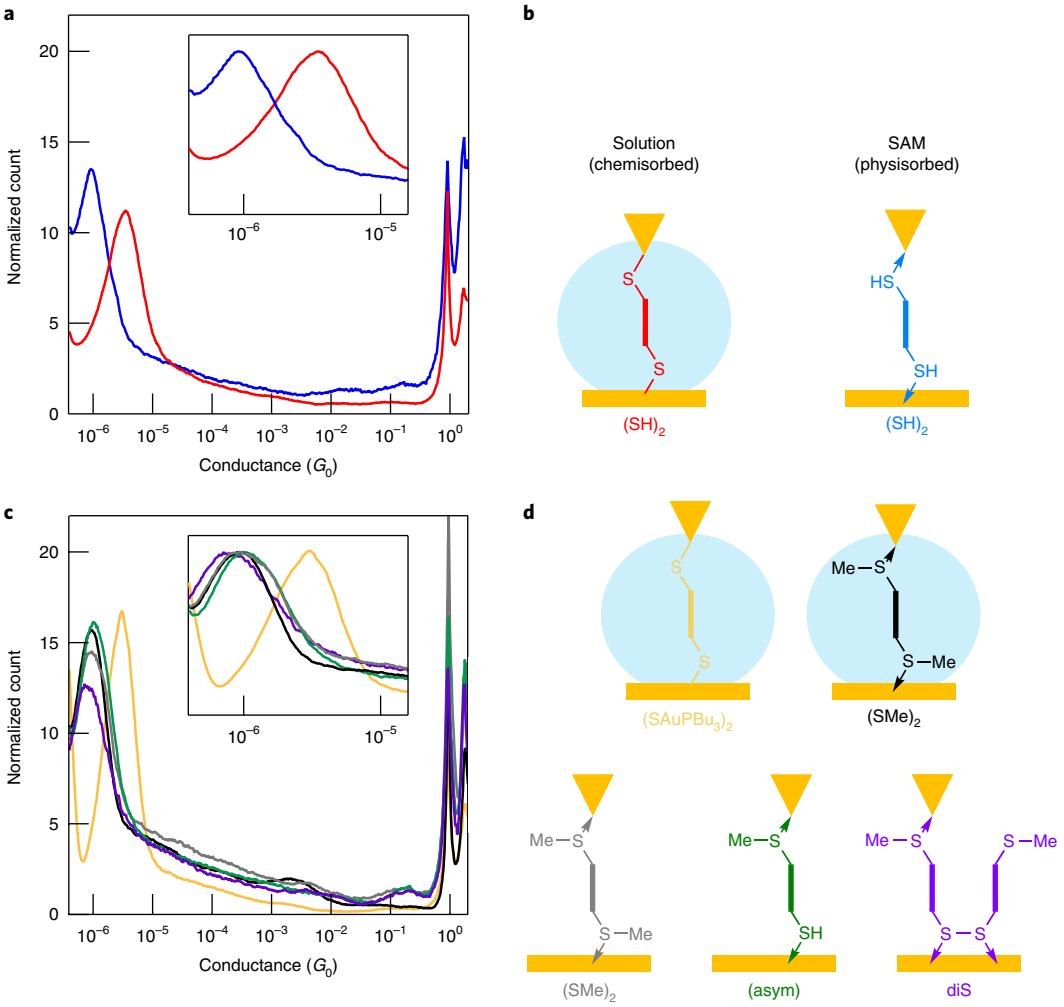

Fig. 1 | Conductance histograms for solution or SAM measurements of C_{12}-based single-molecule junctions that comprise different sulfur terminal groups. **a**,**c**, 1D logarithmically binned conductance histograms (100 bins per decade) generated, without data selection, from 5,000 conductance traces measured at an applied bias of 345 mV. Histograms from the solution measurements are scaled by 0.5 as these typically yield about twice the number of molecular junctions when compared with SAM measurements. Insets: Expansion of the low-conductance regions, with all the histograms scaled to have the same molecular conductance peak height. **b**,**d**, Colour-coded keys for **a** and **c** that show the different single-molecule junctions measured, in which a line between a sulfur atom and gold electrode indicates a chemisorbed contact and an arrow indicates a physisorbed one. Blue shaded circles indicate solution measurements, and their absence indicates SAM measurements (in air). Horizontal yellow bar, gold substrate; yellow triangle, gold tip; **C_{12}(asym)**, an asymmetrically substituted molecule with one –SMe and one –SH linker; **C_{12}(diS)**, a dimer of **C_{12}(asym)** in which the –SH linkers have been oxidized to form a disulfide.

measurements', performed by measuring a SAM of $\mathbf{C_{12}(SH)_2}$ in air, in which the SAMs are first prepared on template-stripped gold substrates using standard techniques (that is, 18–28 hours of immersion in a 1 mM EtOH solution[3]) as detailed in the Methods and Supplementary Information. We hereafter use these two expressions (solution measurements and SAM measurements) in reference to these particular measurement protocols. For $\mathbf{C_{12}(SH)_2}$, solution measurements yield a conductance peak at 3.3×10^{-6} G_0 (Fig. 1a, red), whereas SAM measurements yield a conductance peak at 9.0×10^{-7} G_0 (Fig. 1a, blue). As described previously[21], SAM measurements are otherwise identical to those performed in solution, both starting with the formation of a gold point contact, except that in SAM measurements the tip is regularly moved laterally relative to the substrate to avoid depleting the local area of molecules.

We postulate that these observed differences in conductance arise from different bonding interactions between sulfur and gold: in solution measurements, the conductance is consistent with the thiol functionality being chemisorbed on gold and the hydrogen being lost on bond formation (that is, Au–SR); in contrast, in SAM measurements, the conductance is consistent with the thiol being physisorbed, with no loss of hydrogen. A gold–sulfur physisorbed interaction (sometimes referred to as, but not necessarily synonymous with, a donor–acceptor, coordination or dative interaction) is one in which the hydrogen is not lost, so there is no significant chemical change to the molecular species on interaction with the surface (Fig. 1b)[22]. The sensitivity of single-molecule junction conductance with respect to the electrode–molecule contact is well established[23,24]. To test this hypothesis, we ran a series of additional STM-BJ conductance measurements of the C_{12} (dodecane) backbone terminated with different sulfur-based linkers (Supplementary Tables 1–3 give an overview of all the measurements and conditions). Unlike solution measurements of $\mathbf{C_{12}(SH)_2}$, solution measurements of $\mathbf{C_{12}(SMe)_2}$ (Fig. 1, black, 9.1×10^{-7} G_0) yield roughly the same conductance peak as the SAM measurement of $\mathbf{C_{12}(SH)_2}$ and $\mathbf{C_{12}(SMe)_2}$ (Fig. 1, blue, 9.0×10^{-7} G_0 and grey, 9.7×10^{-7} G_0). As the thioether moiety in $\mathbf{C_{12}(SMe)_2}$ can only bind to gold via a physisorbed contact, this result supports the conclusion that gold–sulfur bonds in the $\mathbf{C_{12}(SH)_2}$ SAMs are also of a physisorbed, and not

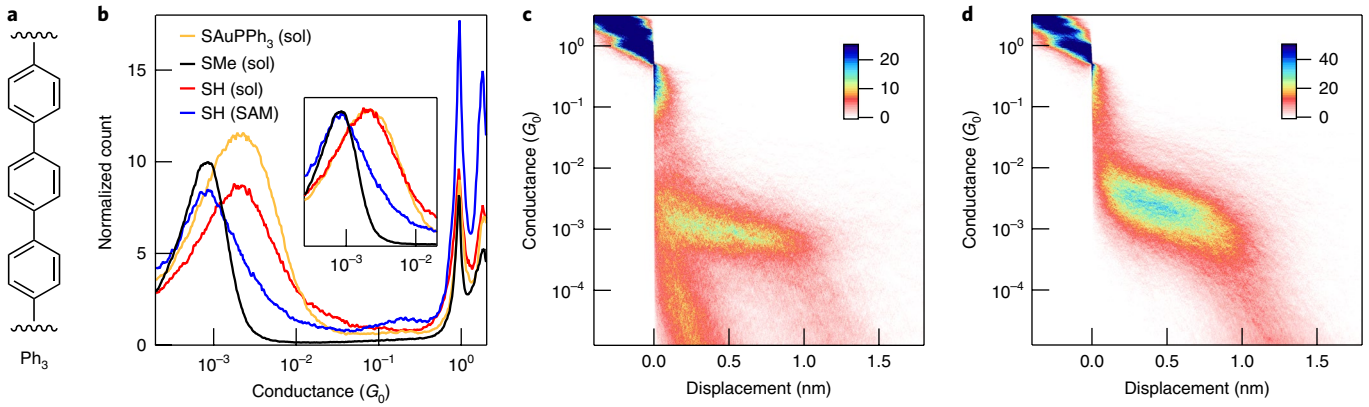

Fig. 2 | Conductance histograms for terphenyl (Ph_3)-based single-molecule junctions that comprise different sulfur terminal groups. a, Molecular structure for the Ph_3 backbone. **b**, 1D logarithmically binned conductance histograms (100 bins decade^{-1}) generated, without data selection, from 5,000 conductance traces measured at an applied bias of 230 mV. Histograms from the solution measurements are scaled by 0.5. Inset: Expansion of the low-conductance region, with all the histograms scaled to have the same molecular conductance peak height. **c**,**d**, 2D conductance–displacement histograms of **$Ph_3(SH)_2$** SAM (**c**) and solution (**d**) measurements. These histograms are created by aligning all the measured traces to zero displacement at 0.5 G_0 and using 100 bins decade^{-1} along the conductance axis and 400 bins nm^{-1} along the displacement axis. The colour bar indicates the number of counts. **$Ph_3(SH)_2$** solution measurements give broader conductance distributions, as expected due to the varied binding motifs for a chemisorbed gold–sulfur bond when compared with a physisorbed one.

chemisorbed, gold–sulfur character. We attribute the higher conductance of **$C_{12}(SH)_2$** in solution measurements to the molecule binding to gold through chemisorbed contacts at both termini.

To confirm this interpretation, we synthesized **$C_{12}(SAuPBu_3)_2$**, a complex that comprises the same C_{12} backbone but with pre-installed covalent gold–thiolate bonds. Solution measurements of such systems have previously been shown to form junctions through the Au(I) atom of the complex, and in this case ensure that the junctions comprise chemisorbed gold–sulfur bonds[25]. We obtained a conductance value of $3.0\times10^{-6}\,G_0$ for solution measurements of **$C_{12}(SAuPBu_3)_2$** (Fig. 1, yellow), very close to that of the solution measurement of **$C_{12}(SH)_2$** (Fig. 1, red). We also considered a SAM measurement of an asymmetrically terminated C_{12} alkane with a thiol (–SH) linker on one end and a thioether (–SMe) on the other (**C_{12}(asym)**), as shown in Fig. 1 (green). A SAM measurement of this molecule yielded the same conductance ($1.0\times10^{-6}\,G_0$) as the SAM measurement of **$C_{12}(SH)_2$**. Additionally, a SAM measurement of **C_{12}(diS)**, a disulfide terminated with thioether groups (that is, MeS–C_{12}–S–S–C_{12}–SMe), yielded a conductance peak at $8.0\times10^{-7}\,G_0$ (Fig. 1, purple). In summary, as clearly indicated in Fig. 1, we observed a low conductance for all the measured C_{12} systems with double physisorbed contacts. We observed a high conductance only for solution measurements of **$C_{12}(SH)_2$** and **$C_{12}(SAuPBu_3)_2$**, which we attribute to having double chemisorbed contacts.

Similar results were also found with 1,10-decanedithiol (**$C_{10}(SH)_2$**) and 1,8-octanedithiol (**$C_8(SH)_2$**), as shown in Supplementary Fig. 1, which illustrates that these effects are not specific to the C_{12} backbone. However, we note that as the alkane backbone length is made shorter, the difference in conductance between the SAM and solution measurements decreases. This finding, along with the fact that we see single peaks (rather than double or multiple peaks), rules out the possibility that we are measuring multiple molecular junctions in solution measurements and single-molecule junctions in SAM measurements. Additionally, we do not observe a change in conductance for $C_{12}(SH_2)$, **C_{12}(asym)** or **$C_{12}(SMe)_2$** solution measurements at lower concentrations (Supplementary Fig. 2). This conclusion is further supported by the fact that we see no difference in conductance between the SAM and solution measurements of **$C_{12}(SMe)_2$** (Fig. 1c). We must stress the importance of the remarkable differences observed by these single-molecule measurements in this study, which probe the modes of binding between molecules of **$C_{12}(SH)_2$** and gold as a function of charge transport. The STM-BJ data provide detail on molecular interactions; such differences have not been observed through other experimental techniques[14–19].

Finally, as additional controls we used different solvents, added a solvent on top of a SAM prior to the STM-BJ SAM measurements, varied the SAM preparation conditions and reversed the bias polarity, all of which reinforced our hypothesis (see Supplementary Fig. 3 and Supplementary Tables 1–3 for an overview of all the measurements and conditions). In every case, the conductance of a SAM measurement of an SH-terminated molecule did not increase to that of a solution measurement. These experiments serve to exclude further the effects of the solvent/molecular environment, substrate surface roughness, nanoscale SAM structure or thiol oxidation on the observed conductance differences between the SAM and solution measurements. Based on the results presented in Fig. 1, we can therefore conclude that alkanethiols in SAMs prepared from solution deposition are not chemisorbed, but rather are physisorbed on the gold surface.

To test whether the differences seen with **$C_{12}(SH)_2$** can be attributed to differences between saturated and conjugated SAMs, similar measurements were carried out with terphenyl analogues (Ph_3, see Fig. 2a) in which the backbones are terminated symmetrically with –SH, –SMe or –$SAuPPh_3$ linkers. Figure 2b shows the conductance histograms for solution measurements of all three molecules as well as a SAM measurement of **$Ph_3(SH)_2$**. The results are consistent with those for C_{12}. Solution measurement of the dithiol yields a conductance that is higher than that of the SAM measurement. We also found that the conductance of a **$Ph_3(SH)_2$** SAM measurement is the same as that for the **$Ph_3(SMe)_2$** solution measurement and that the **$Ph_3(SH)_2$** solution measurement yields the same conductance as the **$Ph_3(SAuPPh_3)_2$** solution measurement. To illustrate further the difference between the SAM and solution measurements of **$Ph_3(SH)_2$**, we compare in Fig. 2c,d two-dimensional (2D) conductance histograms that show how the junction conductance varies with increasing tip–substrate separation (elongation). Although both exhibit a feature with the same length, for the SAM measurement we see a horizontal feature (the junction conductance does not vary significantly with junction elongation), whereas the solution measurement shows a sloped one. Such differences are also observed in 2D histograms for the saturated systems (Supplementary Fig. 4). This provides a further indication of physisorbed bonding in the

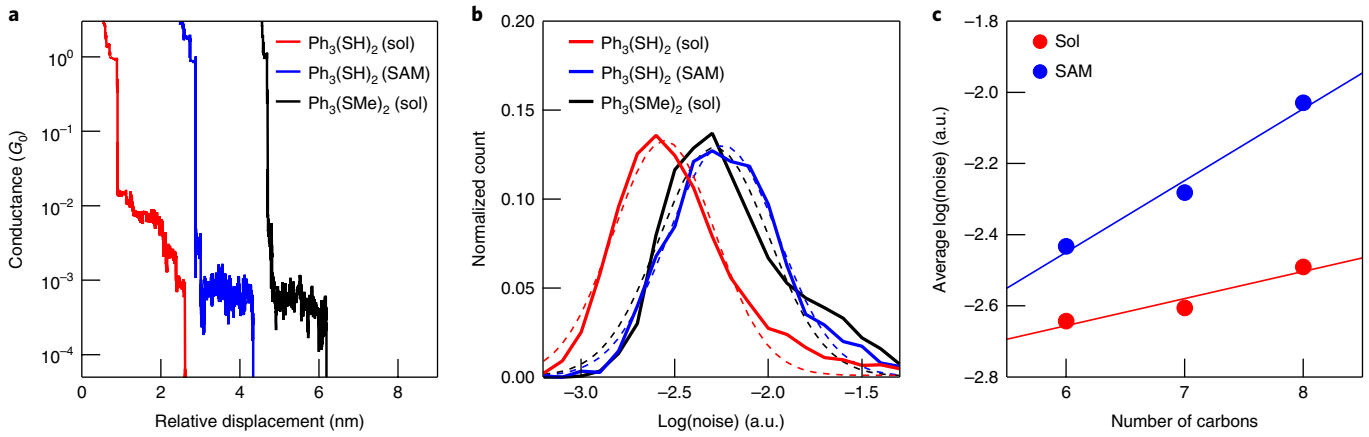

Fig. 3 | Noise analysis for Ph_3- and C_n-based single-molecule junctions. a, Representative individual traces for **$Ph_3(SH)_2$** SAM and **$Ph_3(SMe)_2$** and **$Ph_3(SH)_2$** solution measurements. **b**, Overlaid normalized histograms of the average conductance noise for molecules with Ph_3 backbones (solid lines) and their Gaussian fits (dotted lines). **c**, A plot of the average conductance noise for the SAM and solution measurements of $C_n(SH)_2$ for $n = 6$, 7 and 8. Values are obtained by Gaussian fits to the corresponding conductance noise histograms (Supplementary Fig. 5). Lines are linear fits to the data. This analysis demonstrates that junctions formed from the solution measurements of SH-terminated molecules (chemisorbed) exhibit a smaller conductance noise than those from the SAM measurements (physisorbed). The junction noise of **$Ph_3(SH)_2$** in the SAM measurements is comparable to that of the solution measurements of **$Ph_3(SMe)_2$**, which offers a further indication that the molecule–electrode bonding is similar in both cases (both physisorbed). The errors in the Gaussian fits are smaller than the markers used to denote the values. a.u., arbitrary units.

SAM measurements of dithiols in contrast to the solution measurements[26], as physisorbed species bind predominantly to undercoordinated gold adatoms[27] (a well-defined configuration), whereas chemisorbed thiols can adopt multiple contact geometries (different linker configurations on elongation)[26,28,29]. The impact of junction configurations on conductance is discussed in more detail below. The Ph_3 measurements demonstrate that the observed phenomenon is not unique to alkane backbones, and further implicate the electrode–molecule gold–sulfur bond as responsible for the observed differences between the conductance of thiols in SAM and solution measurements. Taken together, these measurements provide strong evidence that thiols do not form chemisorbed bonds in SAMs, and that, instead, this bonding interaction is of a physisorbed character.

Conductance noise analysis. We next analysed individual conductance traces to illustrate further differences between physisorbed and chemisorbed molecular junctions. It has been shown that molecular junctions formed with stronger metal–molecule links are less susceptible to conductance fluctuations than those formed with weaker ones[30,31]. We therefore compare conductance noise for molecular junctions from both SAM and solution measurements. Figure 3a shows sample conductance traces measured for Ph_3, where it is evident that the molecular junction conductance fluctuations (on a logarithm scale) are larger for the **$Ph_3(SH)_2$** SAM and **$Ph_3(SMe)_2$** solution measurements when compared to the **$Ph_3(SH)_2$** solution measurement. To quantify the conductance noise across different molecular junctions, we determined the magnitude of the conductance fluctuations relative to the average conductance for molecular conductance steps and looked at the distribution of these differences (normalized to the step length) across different junctions. The analysis details are presented in the Methods and Supplementary Information. Figure 3b shows logarithmically binned histograms of conductance noise for the three different Ph_3 measurements. We found that the noise distributions are nearly identical for the **$Ph_3(SMe)_2$** solution and **$Ph_3(SH)_2$** SAM measurements, whereas the noise for the **$Ph_3(SH)_2$** solution measurements is clearly lower. To see if the difference between a solution and SAM measurement is also observed for alkanes, we repeated the same analysis for **$C_6(SH)_2$**, **$C_7(SH)_2$** and **$C_8(SH)_2$**. We found again that the noise is smaller for solution measurements when compared with SAM measurements, and reproduced a length-dependent noise that was found previously[30]. These analyses confirm a clear difference in the bonding at the gold–sulfur interface in SAM measurements of SH-terminated molecules (physisorbed) in comparison to the solution measurements (chemisorbed).

Transport calculations. We now turn to ab initio calculations to rationalize the trends in the measured single-molecule conductance of alkanes with different gold–sulfur linkers. We employed a DFT-based non-equilibrium Green's function approach, with the TranSIESTA package[32] as described in the Methods and Supplementary Methods. We note that, although commonly used functionals cannot capture conductance values quantitatively[33,34], the trends across families and linker groups are accurate[35], as is also confirmed by our calculations here. In Fig. 4a, we plot the calculated transmission functions for C_{12} alkanes bound to extended gold electrodes with physisorbed Au–S(H)R and Au–S(Me)R as well as with chemisorbed Au–SR with the thiol hydrogen explicitly removed (Supplementary Figs. 6 and 7 show sample geometries and their justification). The DFT-based transmission of Au–S(H)R (Fig. 4a, blue) and Au–S(Me)R (Fig. 4a, black) bonded junctions are very similar over a 6 eV energy window around the Fermi energy, E_F. Small differences arise only in the energy range associated with the unoccupied states, above E_F. The DFT transmission for the Au–SR (Fig. 4a, red) bonded junction, however, is quite distinct and yields a transmission at E_F that is about seven times larger than those of the other two junctions. The higher conductance can be attributed to a resonance peak energy closer to E_F, at around −2.5 eV, and an Au–SR bond gateway state with a peak energy at around −1.1 eV. Note that the gold triad junction structure is chosen to model STM-BJ measurements[28,36] and not to represent the exact atomic details of the molecule–Au interface in a SAM. Additional calculations that utilize an adatom motif yield similar trends (Supplementary Fig. 8). We stress that, although the measured conductance and calculated transmission data presented here for SAMs relate to a molecule–electrode interface that has been disrupted from its equilibrium configuration by STM-BJ measurements, our experiments and calculation geometries nonetheless provide valuable information regarding the equilibrium bonding configuration of the thiol functionality on the gold surface (that is, whether the thiols are chemisorbed or physisorbed in a SAM).

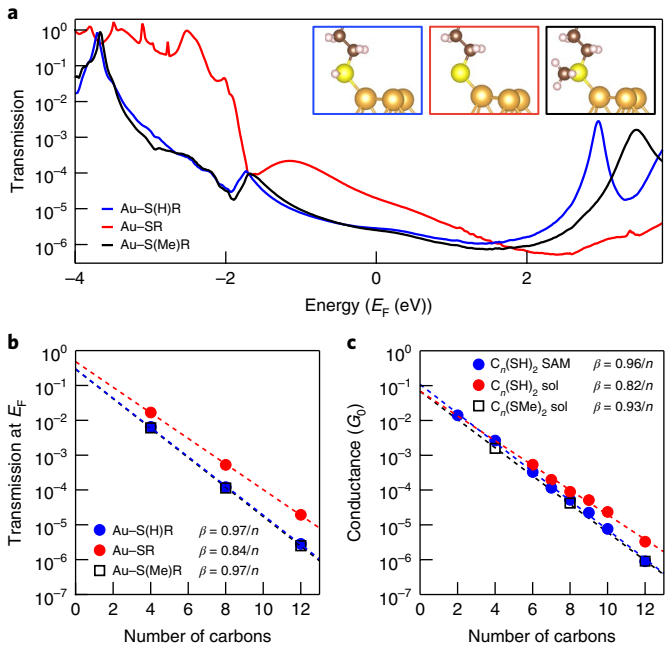

Fig. 4 | Calculated transmission and measured conductance for alkanes with terminal sulfur groups. a, Calculated transmission functions for C_{12} alkanes with Au-S(H)R (blue), Au-SR (red) and Au-S(Me)R (black) bonds as illustrated in the insets (for the molecular structure: Au, gold; S, yellow; C, black; H, white). Peaks that correspond to gateway states for the Au-SR bonded junction are observed at approximately -1.1 eV. The peaks at around -1.8 eV in the other two transmissions are due to the Au *d* states. **b**, The calculated conductance (transmission at E_F) for a series of alkanes with Au-S(H)R (blue), Au-SR (red) and Au-S(Me)R (black) bonds as a function of the number of carbons in the backbone on a semilogarithmic scale. Exponential fits (dashed lines) indicate that the conductance decays for the Au-S(H)R and Au-SR bonded junctions are different. **c**, The conductance histogram peak values for $C_n(SH)_2$ SAM, $C_n(SH)_2$ solution and $C_n(SMe)_2$ solution measurements plotted versus the number of carbons (n) on a semilogarithmic scale. Exponential fits (dashed lines) reveal similar β values for the $C_n(SH)_2$ SAM and $C_n(SMe)_2$ solution measurements, and a lower β value for the $C_n(SH)_2$ solution measurements.

To compare the trends in conductance for alkanes of different lengths, we calculated the transmission for Au–S(H)R, Au–SR and Au–S(Me)R bonded C_4 and C_8 junctions (Supplementary Fig. 9). In Fig. 4b, we plot the zero-bias transmission at E_F as a function of the number of carbons (n) in the backbones on a semilogarithmic scale. The Au–SR bonded junctions are calculated to have a decay parameter of $\beta = 0.84/n$, whereas Au–S(H)R and Au–S(Me)R junctions have $\beta = 0.97/n$. We show the conductance histogram peak values for alkanes of different lengths obtained from SAM (with –SH termini) and solution (–SMe and –SH termini) measurements in Fig. 4c (Supplementary Fig. 10 gives the raw data). The measured trends in these decay factors are in excellent agreement with our calculations. Specifically, we found that chemisorbed junctions (–SH solution measurements) exhibit a slower decay in comparison to the physisorbed junctions (–SH SAM and –SMe solution measurements).

Electrochemistry and XPS. SAMs prepared using identical methods were further characterized by surface cyclic voltammetry and XPS. Here, 1-dodecanethiol (**C_{12}SH**) SAMs exhibited a S 2*p* doublet at a binding energy of ~162 eV, and reductive desorption events below about –1 V (Supplementary Figs. 11 and 12). These are both typical features of SAMs formed from thiols on gold, and have been historically interpreted as characteristic of chemisorbed gold–sulfur bonding[3,5,37]. Remarkably, we found that SAMs formed from *n*-dodecyl methyl sulfide (**C_{12}SMe**) show an indistinguishable XPS binding energy and a similar voltammetric response (Supplementary Figs. 11 and 12), even though this molecule cannot form chemisorbed gold–sulfur bonds. Similar observations have been made in other thioether- and thiophene-bound SAMs[38–40], although it has also been cautioned that adventitious solution-based impurities can severely complicate such measurements[41]. In any case, these features may not reliably be used to explicitly distinguish between chemisorbed and physisorbed molecule–surface bonding in SAMs prepared via solution deposition. Additionally, we note that these techniques are restricted to probing macroscopic surface characteristics, whereas the STM-BJ technique can be applied to study surfaces areas of ~50 nm² (ref. [42]).

Impact of junction configurations. We conclude by ruling out the possibility that the different conductance values observed here between the solution and SAM measurements can be attributed to the different conductance states found for alkanedithiol molecular junctions in previous works[17,43,44]. As an example, in Li et al., junctions with chemisorbed contacts were categorized into three different molecule–electrode binding configurations: 'high', attributed to bridging gold–sulfur contacts with an all-*trans* alkane backbone, 'medium', with atop contacts with an all-*trans* backbone, and 'low' attributed to atop contacts with a single gauche backbone defect[17]. In our work, we cannot categorize SAM-based junctions to one chemisorbed binding configuration and solution-based ones to another. We arrive at this conclusion following seven points. (1) Any such sorting attributed to our SAM or solution data must apply to all $C_n(SH)_2$ molecules studied, as we find a clear exponential length dependence for the measured conductance in the SAM and solution measurements (Fig. 4c). (2) The histograms shown here are constructed from thousands of individual conductance traces without data selection. Our measurement process naturally samples different junction configurations with a range of different conductance values that contribute to the histogram peak widths. (3) The measured conductance values obtained here for all $C_n(SH)_2$ solution measurements generally agree with the values assigned to the medium group[17,18,30], which shows that the junctions formed in the $C_n(SH)_2$ SAM measurements must be in a lower conducting junction configuration than one with chemisorbed atop contacts and an all-*trans* backbone. This interpretation is supported by the negligible overlap between the conductance peaks obtained from the SAM and solution measurements for **$C_{12}(SH)_2$** (Fig. 1a). (4) Calculations have shown that for chemisorbed thiols, the atop gold–sulfur binding geometry provides the lowest conductance (medium group)[17]. Therefore, the only available remaining junction configuration that could explain the lower conductance in the SAM measurements is the low group with atop contacts and a single gauche defect. Such defects result in alkane backbone conformations that are shorter in length and exhibit reduced vicinal electronic coupling. However, it is implausible to have gauche defects only in the SAM measurements and not in the solution measurements, and an analysis of our 2D histograms clearly indicates that the junction elongation length is similar in each case (Supplementary Fig. 4). Additionally, the conductance values measured previously for the low group are substantially lower than the values we obtained here for the SAM measurements (for example, 3.2×10^{-5} G_0 for **$C_6(SH)_2$**)[17]. Any hypothesis based on alkane backbone gauche defects also cannot explain the similar behaviour observed with sulfur-terminated molecules that comprise a rigid, conjugated terphenyl backbone (Fig. 2). We must therefore rule out the possibility that the SAM measurements presented here correspond to chemisorbed junction configurations associated with the high, medium or low conductance groups that have been observed before. (5) We find excellent

agreement between the conductance measured: (i) for $\mathbf{C_{12}(SAuPBu_3)_2}$ (with pre-installed gold–thiolate bonds) and $\mathbf{C_{12}(SH)_2}$ solution measurements, (ii) for $\mathbf{C_{12}(SMe)_2}$ solution measurements (which can only form physisorbed contacts) and $\mathbf{C_{12}(SH)_2}$ SAM measurements and (iii) for $\mathbf{C_{12}(SMe)_2}$ SAM and solution measurements (Fig. 1). (6) Our analysis of conductance noise (Fig. 3) also implicates the nature of the gold–sulfur bond rather than different chemisorbed binding configurations. (7) As a final point, all our measurements start from a gold–gold contact and we do not see a change in conductance in the SAM measurements of $\mathbf{C_{10}(SH)_2}$ when we add solvent on top of the SAM (Supplementary Fig. 3).

Conclusion

Taken together, our STM-BJ measurements demonstrate that SAMs formed on gold surfaces from SH-terminated precursors do not predominantly comprise chemisorbed (or covalent) gold–sulfur bonds. Instead we find that chemisorbed bonds are only consistently formed in solution STM-BJ measurements of thiol-functionalized compounds with gold electrodes. This implies that an excess of molecules around high-energy, undercoordinated surface gold sites is a prerequisite for cleaving the thiol sulfur–hydrogen bond. Although the mechanistic origins of our observations require further clarification, we show that key properties of gold–sulfur SAMs can be better rationalized if the bonding is considered physisorbed in character. For example, both the high mobility of components on gold surfaces, where the gold–sulfur bond is evidently labile[45], and the role that van der Waals interactions play in providing stability to adsorbed layers[10] are consistent with our conclusions. Furthermore, our results provide new insights into several associated questions and observations, which include the mechanism of hydrogen loss on assembly (predominantly, it is not lost in SAMs prepared via solution deposition at room temperature)[46], the poor stability of thiol-based SAMs compared to *N*-heterocyclic carbenes[47] and the multiple 'chemisorbed' peaks in temperature-programmed desorption experiments[48]. By exposing the true nature of gold–thiol bonds in SAMs, this work will help focus efforts to identify new linker groups, and/or preparation methods, that facilitate the construction of more stable SAMs with increased electronic transparency.

Methods

Conductance measurements. Unless otherwise stated, solution measurements were performed after the addition of 0.1 mM analyte solutions in 1,2,4-trichlorobenzene (Sigma–Aldrich or Alfa Aesar, 99% purity) to a clean gold-on-mica or gold-on-steel substrate. SAM measurements were performed on SAMs prepared on the same day. In the SAM measurements, freshly cut gold tips were repeatedly moved laterally relative to the substrate by ≥200 nm after measuring ~250 traces at a given tip–substrate position. This ensured there were always enough molecules to form junctions and also helped to average out local variations across the surface. Conductance histograms were compiled without data selection and typically comprise ≥5,000 consecutively measured traces. The time required to obtain ~5,000 traces in a solution measurement is on the same order as that required to measure the same number of traces in a SAM measurement (1–2 h).

SAM preparation. Unless otherwise stated, freshly cleaved template-stripped gold substrates were immersed in 1 mM solutions of the analyte in absolute ethanol[3]. $\mathbf{Ph_3(SH)_2}$ SAMs were formed using 0.05 mM ethanolic solutions[49]. Substrates were removed after 18–28 h, rinsed copiously with absolute ethanol (≥4×2 ml), and dried in a stream of N_2. Analyte solutions were prepared in glass scintillation vials by successive dilution from more concentrated solutions, starting from pure samples of the analyte material weighed on a microbalance. No attempts were made to exclude air during the SAM preparation. Control experiments using SAMs prepared using argon-sparged solutions under an atmosphere of argon showed that the presence of air does not impact the resulting STM-BJ SAM measurements (Supplementary Fig. 3). No significant changes were observed in additional control studies (for example, varying the preparation solution concentration or solvent, immersion time or substrate type), which demonstrates that the results presented here are broadly independent of the conditions used to prepare the SAMs (Supplementary Fig. 3).

Synthesis of C_{12} asymmetrical alkanes and gold complexes. Starting from symmetrical 1,12-dibromoalkane, –SMe and –SAc terminal groups were introduced through stepwise nucleophilic substitution reactions with NaSMe and KSAc in refluxing THF[50,51] to provide the asymmetrical precursor **2** (Supplementary Information, scheme 2). Subsequent reduction of the terminal –SAc moiety to –SH using $LiAlH_4$ (ref. [51]) yielded $\mathbf{C_{12}(asym)}$. This could be oxidized with NaI–H_2O_2 (ref. [52]) to form the corresponding disulfide ($\mathbf{C_{12}(diS)}$). Symmetrical bis-gold(I) thiolate complexes were prepared with C_{12} and Ph_3 backbones through deprotonation of the corresponding terminal dithiol ($\mathbf{C_{12}(SH)_2}$ or $\mathbf{Ph_3(SH)_2}$) using an appropriate base (KOH or $Cs_2(CO_3)$), followed by reaction with $ClAuPPh_3$ (for example, Supplementary Information, scheme 3)[53,54]. The highly insoluble, probably polymeric, C_{12}-backbone material (**3**) formed in this manner was solubilized using P^nBu_3 immediately prior to conductance measurements[55].

Noise analysis. We analysed all the traces collected, selected those that comprised a molecular junction and then quantified the average conductance noise as follows. We first extracted data points from the region of the conductance trace that corresponds to the molecular junction, that is, when the conductance is within the histogram peak. We took the logarithm of this segment and fit it with a line. If the line fit was highly sloped (corresponding to an exponential decay seen in traces without molecules), we omitted the trace. About 30–60% of the measured traces were selected (the fraction depends on the molecular backbone length and on the measurement conditions, that is, the solution versus the SAM measurements). For each selected trace, we took the difference between the raw and smooth data for all the points that comprised the step feature. The smoothed data were obtained by averaging 11 neighbouring points (as illustrated in Supplementary Fig. 5). These differences were squared and their sum for each trace normalized by the number of points in the selected segment. This constitutes the noise for the trace. We compiled logarithmically binned histograms of this noise parameter for every junction and fit these histograms with a Gaussian function to determine the average noise for that measurement (that is, for each junction type). We note that the absolute value of the noise is specific to the acquisition rate and pulling speed in our custom STM and, thus, although the trends in the noise across different molecular junctions are robust, the actual numbers vary depending on the experimental set-up.

Computational details. We relaxed the junction geometries with DFT using the Perdew–Burke–Ernzerhof functional[56] as implemented in the SIESTA package[57]. We used 4×4 Au atoms on each layer, and seven layers of Au(111) on each side of the molecule. In the junction relaxation, the internal atomic distances within the outmost four layers of Au on each side of the molecule were kept constant at their bulk values. The pseudopotentials and basis sets were adapted from previous work[27]. A single-zeta polarization basis set was used for the Au atoms and double-zeta polarization basis sets were used for other elements. Norm-conserving pseudopotentials were used and, for Au, the pseudopotential and basis set were chosen so as to reproduce the experimental work function of a clean Au(111) surface. A 4×4×1 *k*-mesh was used.

After the junction geometry was relaxed, transport properties were calculated using the non-equilibrium Green's function formalism as implemented in the TranSIESTA package[32] with the same functional, pseudopotentials, basis set, and *k*-mesh as above. The default value of 36 energy points was used in the contour integration. After convergence of the non-equilibrium Hamiltonian, the transmission was calculated using the Landauer formalism with a 16×16 *k*-mesh in a postprocessing step. This work focused on the qualitative trends and the comparison of β values (defined as $G_n = G_c e^{-\beta n}$, where G_n is the conductance of an alkane chain that comprises n carbons and G_c is the contact conductance) between experiment and calculations. Therefore, we did not apply self-energy corrections, such as in previous work[35], and as a result we expect qualitative but not quantitative agreement between the measured and calculated conductance.

Code availability

The data that support the findings were acquired using a custom instrument controlled by custom software (Igor Pro, Wavemetrics). The software is available from the corresponding author upon reasonable request.

Data availability

The data that support the findings of this study not included in the Supplementary Information are available from the corresponding author upon reasonable request.

Received: 16 February 2018; Accepted: 3 January 2019;
Published online: 4 March 2019

References

1. Nuzzo, R. G. & Allara, D. L. Adsorption of bifunctional organic disulfides on gold surfaces. *J. Am. Chem. Soc.* **105**, 4481–4483 (1983).
2. Bain, C. D. & Whitesides, G. M. Molecular-level control over surface order in self-assembled monolayer films of thiols on gold. *Science* **240**, 62–63 (1988).
3. Love, J. C., Estroff, L. A., Kriebel, J. K., Nuzzo, R. G. & Whitesides, G. M. Self-assembled monolayers of thiolates on metals as a form of nanotechnology. *Chem. Rev.* **105**, 1103–1170 (2005).
4. Hakkinen, H. The gold–sulfur interface at the nanoscale. *Nat. Chem.* **4**, 443–455 (2012).

5. Bain, C. D., Biebuyck, H. A. & Whitesides, G. M. Comparison of self-assembled monolayers on gold: coadsorption of thiols and disulfides. *Langmuir* **5**, 723–727 (1989).
6. Cossaro, A. et al. X-ray diffraction and computation yield the structure of alkanethiols on gold(111). *Science* **321**, 943–946 (2008).
7. Walczak, M. M., Alves, C. A., Lamp, B. D. & Porter, M. D. Electrochemical and X-ray photoelectron spectroscopic evidence for differences in the binding sites of alkanethiolate monolayers chemisorbed at gold. *J. Electroanal. Chem.* **396**, 103–114 (1995).
8. Poirier, G. E. & Pylant, E. D. The self-assembly mechanism of alkanethiols on Au(111). *Science* **272**, 1145–1148 (1996).
9. Nuzzo, R. G., Zegarski, B. R. & Dubois, L. H. Fundamental studies of the chemisorption of organosulfur compounds on gold(111). Implications for molecular self-assembly on gold surfaces. *J. Am. Chem. Soc.* **109**, 733–740 (1987).
10. Vericat, C., Vela, M. E., Benitez, G., Carro, P. & Salvarezza, R. C. Self-assembled monolayers of thiols and dithiols on gold: new challenges for a well-known system. *Chem. Soc. Rev.* **39**, 1805–1834 (2010).
11. Pensa, E. et al. The chemistry of the sulfur–gold interface: in search of a unified model. *Acc. Chem. Res.* **45**, 1183–1192 (2012).
12. Reimers, J. R., Ford, M. J., Marcuccio, S. M., Ulstrup, J. & Hush, N. S. Competition of van der Waals and chemical forces on gold–sulfur surfaces and nanoparticles. *Nat. Rev. Chem.* **1**, 0017 (2017).
13. Jadzinsky, P. D., Calero, G., Ackerson, C. J., Bushnell, D. A. & Kornberg, R. D. Structure of a thiol monolayer-protected gold nanoparticle at 1.1 Å resolution. *Science* **318**, 430–433 (2007).
14. Xu, B. & Tao, N. J. Measurement of single-molecule resistance by repeated formation of molecular junctions. *Science* **301**, 1221–1223 (2003).
15. Zhou, C., Muller, C., Burgin, T., Tour, J. & Reed, M. Conductance of a molecular junction. *Science* **278**, 252–254 (1997).
16. Haiss, W. et al. Redox state dependence of single molecule conductivity. *J. Am. Chem. Soc.* **125**, 15294–15295 (2003).
17. Li, C. et al. Charge transport in single Au | alkanedithiol | Au junctions: coordination geometries and conformational degrees of freedom. *J. Am. Chem. Soc.* **130**, 318–326 (2008).
18. Inkpen, M. S. et al. New insights into single-molecule junctions using a robust, unsupervised approach to data collection and analysis. *J. Am. Chem. Soc.* **137**, 9971–9981 (2015).
19. Haiss, W. et al. Anomalous length and voltage dependence of single molecule conductance. *Phys. Chem. Chem. Phys.* **11**, 10831–10838 (2009).
20. Venkataraman, L., Klare, J. E., Nuckolls, C., Hybertsen, M. S. & Steigerwald, M. L. Dependence of single-molecule junction conductance on molecular conformation. *Nature* **442**, 904–907 (2006).
21. Inkpen, M. S., Leroux, Y. R., Hapiot, P., Campos, L. M. & Venkataraman, L. Reversible on-surface wiring of resistive circuits. *Chem. Sci.* **8**, 4340–4346 (2017).
22. Everret, D. H. Definitions, terminology and symbols in colloid and surface chemistry. *Pure Appl. Chem.* **31**, 579–638 (1972).
23. Zang, Y. et al. Electronically transparent Au–N bonds for molecular junctions. *J. Am. Chem. Soc.* **139**, 14845–14848 (2017).
24. Park, Y. S. et al. Contact chemistry and single-molecule conductance: a comparison of phosphines, methyl sulfides, and amines. *J. Am. Chem. Soc.* **129**, 15768–15769 (2007).
25. Cheng, Z. L. et al. In situ formation of highly conducting covalent Au–C contacts for single-molecule junctions. *Nat. Nanotechnol.* **6**, 353–357 (2011).
26. Hybertsen, M. S. & Venkataraman, L. Structure–property relationships in atomic-scale junctions: histograms and beyond. *Acc. Chem. Res.* **49**, 452–460 (2016).
27. Quek, S. Y. et al. Amine–gold linked single-molecule circuits: experiment and theory. *Nano Lett.* **7**, 3477–3482 (2007).
28. Paulsson, M., Krag, C., Frederiksen, T. & Brandbyge, M. Conductance of alkanedithiol single-molecule junctions: a molecular dynamics study. *Nano Lett.* **9**, 117–121 (2009).
29. Kim, Y.-H., Kim, H. S., Lee, J., Tsutsui, M. & Kawai, T. Stretching-induced conductance variations as fingerprints of contact configurations in single-molecule junctions. *J. Am. Chem. Soc.* **139**, 8286–8294 (2017).
30. Rascón-Ramos, H., Artés, J. M., Li, Y. & Hihath, J. Binding configurations and intramolecular strain in single-molecule devices. *Nat. Mater.* **14**, 517–522 (2015).
31. Adak, O. et al. Flicker noise as a probe of electronic interaction at metal–single molecule interfaces. *Nano Lett.* **15**, 4143–4149 (2015).
32. Brandbyge, M., Mozos, J.-L., Ordejón, P., Taylor, J. & Stokbro, K. Density-functional method for nonequilibrium electron transport. *Phys. Rev. B* **65**, 165401 (2002).
33. Koentopp, M., Burke, K. & Evers, F. Zero-bias molecular electronics: exchange-correlation corrections to Landauer's formula. *Phys. Rev. B* **73**, 121403 (2006).
34. Quek, S. Y. et al. Amine–gold linked single-molecule circuits: experiment and theory. *Nano Lett.* **7**, 3477–3482 (2007).
35. Quek, S. Y., Choi, H. J., Louie, S. G. & Neaton, J. B. Length dependence of conductance in aromatic single-molecule junctions. *Nano Lett.* **9**, 3949–3953 (2009).
36. Hybertsen, M. S. et al. Amine-linked single-molecule circuits: systematic trends across molecular families. *J. Phys. Condens. Matter* **20**, 374115 (2008).
37. Widrig, C. A., Chung, C. & Porter, M. D. The electrochemical desorption of *n*-alkanethiol monolayers from polycrystalline Au and Ag electrodes. *J. Electroanal. Chem. Interfacial Electrochem.* **310**, 335–359 (1991).
38. Angelova, P. et al. Chemisorbed monolayers of corannulene penta-thioethers on gold. *Langmuir* **29**, 2217–2223 (2013).
39. Piotrowski, P. et al. Self-assembly of thioether functionalized fullerenes on gold and their activity in electropolymerization of styrene. *RSC Adv.* **5**, 86771–86778 (2015).
40. Noh, J. et al. High-resolution STM and XPS studies of thiophene self-assembled monolayers on Au(111). *J. Phys. Chem. B* **106**, 7139–7141 (2002).
41. Zhong, C.-J., Brush, R. C., Anderegg, J. & Porter, M. D. Organosulfur monolayers at gold surfaces: reexamination of the case for sulfide adsorption and implications to the formation of monolayers from thiols and disulfides. *Langmuir* **15**, 518–525 (1998).
42. He, J. et al. Measuring single molecule conductance with break junctions. *Faraday Discuss.* **131**, 145–154 (2006).
43. Haiss, W. et al. Impact of junction formation method and surface roughness on single molecule conductance. *J. Phys. Chem. C* **113**, 5823–5833 (2009).
44. Li, X. et al. Conductance of single alkanedithiols: conduction mechanism and effect of molecule–electrode contacts. *J. Am. Chem. Soc.* **128**, 2135–2141 (2006).
45. Burgi, T. Properties of the gold–sulphur interface: from self-assembled monolayers to clusters. *Nanoscale* **7**, 15553–15567 (2015).
46. Hasan, M., Bethell, D. & Brust, M. The fate of sulfur-bound hydrogen on formation of self-assembled thiol monolayers on gold: ^{1}H NMR spectroscopic evidence from solutions of gold clusters. *J. Am. Chem. Soc.* **124**, 1132–1133 (2002).
47. Crudden, C. M. et al. Ultra stable self-assembled monolayers of N-heterocyclic carbenes on gold. *Nat. Chem.* **6**, 409–414 (2014).
48. Lavrich, D. J., Wetterer, S. M., Bernasek, S. L. & Scoles, G. Physisorption and chemisorption of alkanethiols and alkyl sulfides on Au(111). *J. Phys. Chem. B* **102**, 3456–3465 (1998).
49. Xie, Z., Bâldea, I., Smith, C. E., Wu, Y. & Frisbie, C. D. Experimental and theoretical analysis of nanotransport in oligophenylene dithiol junctions as a function of molecular length and contact work function. *ACS Nano* **9**, 8022–8036 (2015).
50. Li, H. et al. Extreme conductance suppression in molecular siloxanes. *J. Am. Chem. Soc.* **139**, 10212–10215 (2017).
51. Li, H. et al. Electric field breakdown in single molecule junctions. *J. Am. Chem. Soc.* **137**, 5028–5033 (2015).
52. Kirihara, M. et al. A mild and environmentally benign oxidation of thiols to disulfides. *Synthesis* **2007**, 3286–3289 (2007).
53. Forward, J. M., Bohmann, D., Fackler, J. P. & Staples, R. J. Luminescence studies of gold(I) thiolate complexes. *Inorg. Chem.* **34**, 6330–6336 (1995).
54. Monzittu, F. M. et al. Different emissive properties in dithiolate gold(I) complexes as a function of the presence of phenylene spacers. *Dalton. Trans.* **43**, 6212–6220 (2014).
55. Atsushi, S. et al. Solvent diversity in the preparation of alkanethiol-capped gold nanoparticles. An approach with a gold(I) thiolate complex. *Chem. Lett.* **39**, 319319–319321 (2010).
56. Perdew, J. P., Burke, K. & Ernzerhof, M. Generalized gradient approximation made simple. *Phys. Rev. Lett.* **78**, 1396–1396 (1997).
57. José, M. S. et al. The SIESTA method for *ab initio* order-N materials simulation. *J. Phys. Condens. Matter* **14**, 2745–2779 (2002).

Acknowledgements

We acknowledge discussions with M. L. Steigerwald, G. Lovat, T. Albrecht, Y. R. Leroux and P. Hapiot, and thank M. C. Buzzeo for the use of electrochemical equipment. This research was supported primarily by a Marie Skłodowska Curie Global Fellowship (M.S.I., MOLCLICK: 657247) within the Horizon 2020 Programme. This work was supported in part by the National Science Foundation grants DMR-1507440 and DMR-1807580. The computational work was supported by the US Department of Energy, Office of Basic Energy Sciences, Materials Sciences and Engineering Division, under contract no. DE–AC02–05CH11231, within the Theory FWP. This work was also supported by the Molecular Foundry through the US Department of Energy, Office of Basic Energy Sciences, under the same contract number. Portions of the computational work were performed at the National Energy Research Scientific Computing Center.

Author contributions

M.S.I. and L.V. conceived and led the project. M.S.I. synthesized the compounds and performed STM, XPS and electrochemical experiments. L.V. carried out the noise analyses. Z.-F.L. and J.B.N. undertook first-principles calculations. The paper was written by M.S.I. and L.V. with contributions from all the other authors.

Competing interests

The authors declare no competing interests.

Additional information

Supplementary information is available for this paper at https://doi.org/10.1038/s41557-019-0216-y.

Correspondence and requests for materials should be addressed to M.S.I. or L.V.